IEEE Access
Multidisciplinary | Rapid Review | Open Access Journal

Received January 14, 2020, accepted February 7, 2020, date of publication February 12, 2020, date of current version February 24, 2020.

Digital Object Identifier 10.1109/ACCESS.2020.2973405

Mach-Zehnder Interferometer Sensor Curvature Demodulation Method Based on the Orthogonal Decomposition of Spectral Curves

MINGYAO LIU[1], JINGLIANG WANG[1], YI LIU[1], YUEGANG TAN[1], KANG YUN[1], LIU HONG[1], HAN SONG[1], XIANGSHENG ZENG[2], PING XIA[1], AND ZHAO LI[1]

[1]Wuhan University of Technology, Wuhan 430070, China
[2]Gaussian Optics (Wuhan) Company, Ltd., Wuhan 430200, China

Corresponding author: Jingliang Wang (wangjl0395@163.com)

This work was supported by the General Program of the National Natural Science Fund of Chinese under Grant 51375359.

ABSTRACT This paper proposes a curvature demodulation of Mach-Zehnder interferometer (MZI) sensors based on complete spectral information. An MZI sensor composed of two waist-enlarged single mode fibers (SMFs) was fabricated. To research the spectral characteristics of the sensor under different curvatures, an experimental system was built to load curvature and save spectra. By analyzing the influence of light intensity and wavelength on the curvature fitting accuracy, researchers have found that complete spectral information can express curvature accurately. This paper introduced the concept of orthogonal decomposition to extract complete spectral information. A group of Chebyshev polynomials was chosen as the basis to decompose the spectral curve into a vector (spectral curve decomposition coefficients). A support vector machine improved by a genetic algorithm (GA-SVM) was used to fit the relationship between the spectral curve decomposition coefficients and the curvature. This paper introduces a new accuracy estimation parameter (''equivalent absolute error''), which is used to measure the accuracy of demodulation. The equivalent absolute error of the method proposed in this paper is 0.0022494 m^{-1}, which is superior to other methods. The advantage of this demodulation method is that the curvature is demodulated independently of the spectral information about a particular peak (valley). The demodulation method is applicable to a demodulation process of multiple physical quantities based on spectral information.

INDEX TERMS Mach-Zehnder interferometer sensors, curvature demodulation, orthogonal decomposition, support vector machine.

I. INTRODUCTION

Optical fiber interferometer sensors have been developed over the past few decades, and have been widely used in temperature, strain, pressure and refractive index measurements [1]–[11]. They can be categorized into 4 types: Michelson interferometers, Mach-Zehnder interferometers, Fabry-Perot interferometers, and Sagnac interferometers. Mach-Zehnder interferometers have been widely used in diverse sensing applications due to their advantages [12]–[18]. MZI sensors have two independent light paths: the reference light path and the sensing light path. The variety of surrounding environmental physical quantities changes the propagation mode of the light in the sensing light path; therefore, the transmission spectrum information is changed. An important area of research on MZI sensors is curvature measurement [19]–[25]. Scholars have differing views on the curvature demodulation of MZI sensors. Several reports have shown that the curvature measured by MZI curvature sensors has a certain relationship with the light intensity of the interference spectrum [19], [22]. However, other researchers have found that the curvature has a certain relationship with the wavelength of the interference spectrum [23]–[33]. In view of all that has been mentioned above, researchers may assume that the curvature of MZI sensors is related to the light intensity and wavelength of the interference spectrum. Extracting the complete information in the spectrum and developing an accurate demodulation method

The associate editor coordinating the review of this manuscript and approving it for publication was Md. Selim Habib.

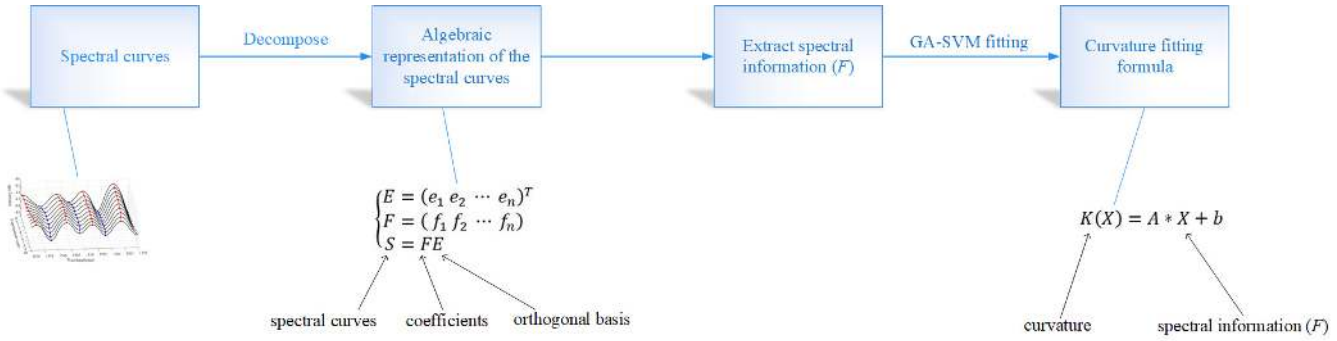

FIGURE 1. MZI sensor curvature demodulation method flow chart.

is an important way to improve the performance of optical fiber interferometer sensors. The spectral information always contains multidimensional data. The general fitting algorithm has difficulty performing multidimensional data fitting. Support vector machines (SVMs) have significant advantages in solving high-dimensional, nonlinear, and other small-sample identification problems or fitting problems [34]–[45]. The purpose of this paper is to construct a curvature demodulation method that adopts complete spectral information. The curvature demodulation method is shown in Fig. 1. First, the spectral curve was decomposed into a vector by the orthogonal base. Then, the complete spectral information was extracted. Finally, the artificial intelligence algorithm was used to fit the spectral information and curvature. The main structure of the study takes the form of three parts, including 'Experiment and Analysis', 'Curvature Demodulation Method' and 'Discussion'. In the first part, an MZI sensor formed by cascading two waist-enlarged single-mode fibers (SMFs) was fabricated. Then, a curvature loading experiment system was set up to obtain the spectral information of the sensor under different curvatures. By comparing the size of the coefficient of determination (R-square) of different fitting forms, the researchers predicted that the fit of combining the light intensity and the wavelength can reflect the spectral information completely. In the second part, the spectral curve was decomposed into a vector (spectral curve decomposition coefficients) based on a group of orthogonal Chebyshev polynomial bases. Next, the support vector machine improved by the genetic algorithm (GA-SVM) was used to fit the correspondence between the spectral curve vector and the curvature. In the third part, the similarities and differences between this study and other studies on the MZI sensor curvature demodulation method were compared. The paper also points out the shortcomings and future research plans of this study.

II. EXPERIMENT AND ANALYSIS

A. SENSOR FABRICATION

Mach-Zehnder interferometers include multiple forms. An MZI sensor that was formed by cascading two waist-enlarged single-mode fibers was fabricated. The detailed

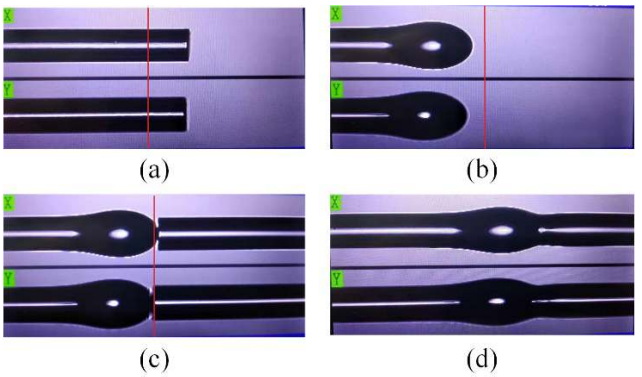

FIGURE 2. Sensor fabrication process: (a) fibers clamping, (b) fiber balls melting, (c) fibers and fiber balls clamping, (d) fibers and fiber balls welding.

fabrication process is illustrated in Fig. 2. First, three single-mode fibers were cut, and their ends were cut flat by a cutter. Two of the fibers (long fiber) were 1 meter long and another (short fiber) was 50 mm long. One of the two long fibers and the short fiber were made of one of the waist-enlarged single-mode fibers. Then, one end of the long fiber was placed on a fusion splicer, and this end was placed beyond the position of the electrode, as shown in Fig. 2(a). Second, the electrode was discharged, and the fiber was melted into a small ball, as shown in Fig. 2(b). Third, one end of the short fiber was placed on the fusion splicer and was aligned to the small ball, as shown in Fig. 2(c). Fourth, the electrode was discharged to fuse the small ball and the short fiber, as shown in Fig. 2(d). The other waist-enlarged single-mode fiber was made as described above. The entire MZI sensor structure is shown in Fig. 3. The length (L) between the two spherical structures was 50 millimeters. The appropriate length (L) was chosen so that the spectrum in the band has the appropriate number of peaks (valleys) [45].

B. EXPERIMENTAL SYSTEM

The experimental system for analyzing the spectral characteristics of the sensor is shown in Fig. 4. The whole experimental system consists of a light source, a spectrum analyzer, single-mode fibers, a sensor, a steel sheet, a height Vernier caliper,

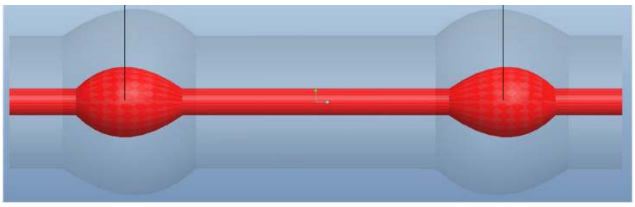

FIGURE 3. Sensor structure.

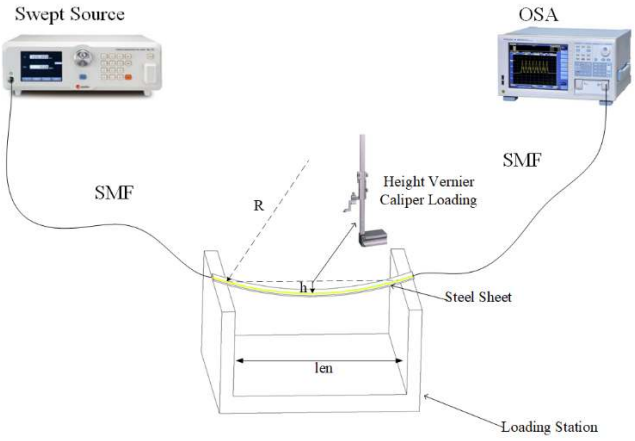

FIGURE 4. Curvature sensing experiment system.

and a loading station. The light source is a broadband light source. The band range is 1530 nm to 1570 nm. Its spectrum sampling interval is 0.01 nm. The sensor was placed in a yellow plastic tube for protection. The yellow plastic tube was attached to the steel sheet. Therefore, the yellow tube and the steel sheet have the same deformation. Additionally, the sensor in the yellow plastic tube was not subjected to the external force. The entire experimental system link sequence is shown in Fig. 4. Here, the steel sheet is a simple beam. When the height Vernier caliper exerts a downward displacement in the middle of the steel sheet, the deformation of the steel sheet is approximately circular. The curvature set by this experimental system can be calculated using:

$$K = \frac{1}{R} = \frac{8h}{len^2 + 4h^2} \tag{1}$$

where K is the curvature, R is the radius of the curvature, len is the length of the loading station, and h is the loading displacement of each experiment.

C. ANALYSIS OF EXPERIMENTS AND RESULTS

The steel sheet was horizontal before the start of the experiment. In this situation, the sensor curvature is 0. Next, the height Vernier caliper was used to exert a downward displacement in the middle of the steel sheet top surface. This displacement was 0.2 mm. Then, 100 experiments were performed. The displacement (h) of each experiment was incremented by 0.2 mm from the previous one. The experimental order with a curvature of zero was 1. During the experiment, the loading station was placed in a temperature control box to ensure that the sensor was not affected by temperature.

TABLE 1. The grouping.

Group order	Experiment order
group 1	1-10
group 2	11-22
group 3	23-32
group 4	33-40
group 5	41-55
group 6	56-70
group 7	71-101

The noise affecting the experiment mainly includes: temperature noise, laser noise and circuit shot noise. Temperature noise is the main noise, and the effects of other noise sources can be ignored. Temperature can affect the optical path difference of the interferometer optical path. It can also affect the cavity length and detector in a laser. To obtain the relationship between the spectra and curvature, a series of studies was performed. First, to exclude noise data, this study performed a wavelet domain denoising on the spectral data of each experiment. Next, the experimental data were divided into 7 groups (the grouping is shown in Table 1) according to the shape of the spectral curve. The experimental results are shown in Fig. 5. The peaks are represented by red lines and the valleys are represented by blue lines.

From Fig. 5, it can be seen that each group has a similar shape. This phenomenon indicates that the spectral curves of each group are the result of similar light propagation mode coupling. This is also the reason for the aforementioned grouping. For the purpose of analysis, the following treatment was performed for each group of spectral curve data (the light intensity and the wavelength to each peak or valley). The curvature (K) of each spectral curve subtracts the curvature value of the first spectral curve. The same treatment was performed for the light intensity (G) and wavelength (W). Then, those relative quantities were fitted with a linear relationship (ΔK to ΔW, ΔG). The fitting formula is shown in Equation 2. Some abbreviations and their meanings are shown in Table 2. The coefficients of determination (R-square) of group 1 are shown in Table 3. The data trends of the other groups are similar to those of group 1.

$$\Delta K = \alpha \times \Delta W + \beta \times \Delta G + \gamma \tag{2}$$

From Table 3, it can be seen that the size relationship between the R-square of 'Only α' and 'Only β' is uncertain. However, the R-square of 'α and β' is larger than the R-square of 'Only α' and 'Only β', respectively. It is surprising that the R-square value of 'α and β' is high and stable. However, this result has not previously been described. This finding is unexpected and suggests that the curvature value of this MZI sensor is determined by the wavelength, light intensity or other quantities of their spectral curve. With further speculations,

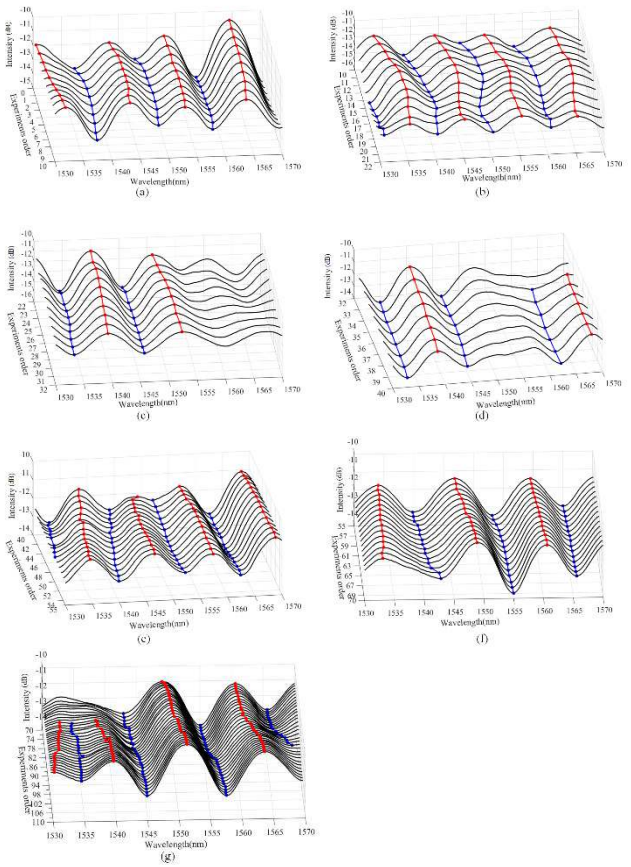

FIGURE 5. Spectral curves: (a) spectral curves of group 1, (b) spectral curves of group 2, (c) spectral curves of group 3, (d) spectral curves of group 4, (e) spectral curves of group 5, (f) spectral curves of group 6, (g) spectral curves of group 7.

TABLE 2. Some abbreviations and their meanings.

Abbreviation	Meaning
Only α	The fitting relationship is only fitted by the wavelength change (ΔW).
Only β	The fitting relationship is only fitted by the light intensity change (ΔG).
α and β	The fitting relationship is fitted by the wavelength drift (ΔW) and the light intensity change (ΔG).

TABLE 3. The coefficient determinations (R-square) of group 1.

Fitting point	Only α	Only β	α and β
Peak1	0.9906	0.3678	0.9933
Peak2	0.009284	0.9802	0.9839
Peak3	0.2624	0.6349	0.744
Peak4	0.3237	0.9814	0.9914
Valley1	0.1148	0.7886	0.9667
Valley2	0.2878	0.2457	0.8887
Valley3	0.3918	0.9704	0.9893

the curvature value measured by this MZI sensor is closely related to the complete information of its spectral curve.

TABLE 4. The order of the orthogonal bases.

Group order	Fitting order
group 1	23
group 2	26
group 3	26
group 4	22
group 5	23
group 6	23
group 7	23

III. CURVATURE DEMODULATION METHOD

The new method of curvature demodulation comprises two steps. These are the orthogonal decomposition of spectral curves and the fitting from spectral information to curvature.

A. ORTHOGONAL DECOMPOSITION OF SPECTRAL CURVES

To extract the complete information of a spectral curve, the spectral curve should be decomposed by a group of orthogonal bases. The coefficients of the orthogonal bases can reflect the complete information of the spectral curve. The Chebyshev polynomials are a group of orthogonal polynomials. The form of these orthogonal polynomials is simple. This advantage makes it the best orthogonal basis for spectral curve decomposition. The form of the Chebyshev polynomial is shown in Equation 3.

$$\begin{cases} T_1 = 1 \\ T_2(x) = x \\ T_{n+1}(x) = 2xT_n(x) - T_{n-1} \quad .(x) \\ |x| \leq 1 \\ n = 2, 3, \cdots \end{cases} \tag{3}$$

The calculation method of the orthogonal basis order about the spectral curve is as follows. First, the wavelengths of each spectral curve in one group were compressed into the interval $[-1,1]$ while the light intensity was unchanged. The new data were equally spaced in the interval $[-1,1]$. Second, the processed data were fitted with Chebyshev polynomials as a basis, and the fitted coefficients of determination were calculated. The Chebyshev polynomial order to be fitted was sequentially increased, and the R-square of each fitting was calculated separately, where the fitting R-square of each spectral curve in one group is greater than 0.999, and the minimum Chebyshev polynomial fitting order is the order of the orthogonal bases to all the spectral curves in the group. The order of the orthogonal bases to all the spectral curves in each group is shown in Table 4.

The specific steps of the spectral curve decomposition method are as follows. First, the wavelengths of each spectral curve in one group were compressed into the interval $[-1,1]$ while the light intensity was unchanged. Second, the researchers established a group of orthogonal bases (E with best fitting order) suitable for each spectral

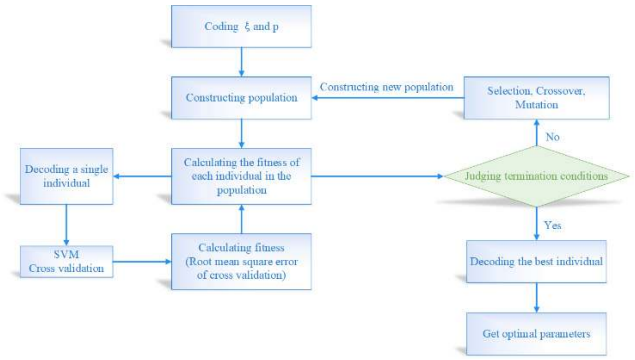

FIGURE 6. Flow chart of the SVM parameter optimization selection algorithm.

curve about the corresponding group. Finally, each spectral curve was fitted using its respective orthogonal basis by least squares, and the coefficients (F) were calculated. These coefficients (F) are the vectors (the spectral curve decomposition coefficients) mentioned above. The form of each spectral curve (S) is shown in Equation 4:

$$\begin{cases} E = (e_1 e_2 \cdots e_n)^T \\ F = (f_1 f_2 \cdots f_n) \\ S = FE \end{cases} \tag{4}$$

Each component e_i of E is the i-th order of the Chebyshev polynomial, and its independent variable range is [−1,1]. Each component f_i of F is a coefficient corresponding to the basis e_i. The coefficients (F) for each spectral curve contain the complete information for that spectrum, including wavelength and light intensity.

B. THE FITTING FROM SPECTRAL INFORMATION TO CURVATURE

From Equation 4, it can be seen that each spectral curve has many fit coefficients. The general fitting algorithm has difficulty performing multidimensional data fitting. Support vector machines (SVMs) have significant advantages in solving high-dimensional, nonlinear, and other small-sample identification problems or fitting problems. In this paper, the support vector machine uses the genetic algorithm to optimize related parameters, which is used to fit multidimensional data. The flow chart of the parameter optimization selection algorithm is shown in Fig. 6. The ε-SVR is used to fit the coefficients (F) and the curvature. The parameters optimized using genetic algorithms are the penalty factor (ξ) and the loss function parameter of ε-SVR (p).

The kernel function ($\kappa(\boldsymbol{x}, \boldsymbol{x}_i)$) chosen in this paper is the linear kernel function. The fitting formula of the support vector machine can be expressed as:

$$f(x) = \sum_{i=1}^{m} \alpha_i \kappa(x, x_i) + b \tag{5}$$

where $\boldsymbol{x}$ is the vector (the spectral curve decomposition coefficients), m is the number of support vectors, x_i is the corresponding support vector, α_i is the coefficient of the corresponding support vector, and b is the offset term. After a series of operations were performed, the final curvature fitting formula was calculated. The expression is:

$$\begin{cases} K(X) = coef\ (UX) + b \\ U = \begin{bmatrix} u_{11} & u_{12} & \cdots & u_{1n} \\ u_{21} & u_{22} & \cdots & u_{2n} \\ \vdots & \vdots & \vdots & \vdots \\ u_{m1} & u_{m2} & \cdots & u_{mn} \end{bmatrix} \\ X = \begin{bmatrix} x_1 & x_2 & \cdots & x_n \end{bmatrix}^T \\ coef = \begin{bmatrix} cf_1 & cf_2 & \cdots & cf_m \end{bmatrix} \end{cases} \tag{6}$$

where X is the vector of spectral curve coefficients (F), n is the dimension of X, m is the number of support vectors, U is the support vector matrix, $coef$ is the matrix of support vector coefficients, and b is the offset term. Equation 6 is rewritten as Equation 7. Equation 7 illustrates the fitting relationship from spectral information to curvature.

$$K(X) = AX + b \tag{7}$$

C. ACCURACY OF THE METHOD

After a series of operations were performed, the absolute error of each experiment (which is shown in Fig. 7) was calculated. The relative error distribution is shown in Fig. 8. The length of the separated relative error interval is 0.1%. The R-square and the average of the relative error absolute value of each group are shown in Fig. 9.

To compare the advantages and disadvantages of this method in similar studies, the author introduces the parameter M("Equivalent Absolute Error"). The expression of M is:

$$M = \frac{1}{n} \sum_{i=1}^{n} |m_i| \tag{8}$$

where i is the experimental order and m_i is the absolute error in the i-th experiment. The authors calculated the parameters M of this article and reference [19], respectively: they are 0.0022494 m^{-1} and 0.0091923 m^{-1}. The lower the value of this parameter, the higher the accuracy is.

It can be seen from the data in Fig. 8 that the relative error is mainly (70%) concentrated in the interval [−0.35%, 0.35%]. As seen from Fig. 9, the R-square value in the seven groups of data is greater than 0.998, except for the smallest group, group 3, whose value is 0.991634. The average of the relative error absolute value of each group decreases as the curvature felt by the sensor increases. The conclusion of the above analysis is that the accuracy of curvature demodulation of the MZI sensor is increased by the combination of orthogonal decomposition and the GA-SVM.

IV. DISCUSSION

Previous studies demodulating the curvature of Mach-Zehnder interferometer curvature sensors have presented differing views. Some reports have shown that the curvature is linear with light intensity [19], [22]. Other

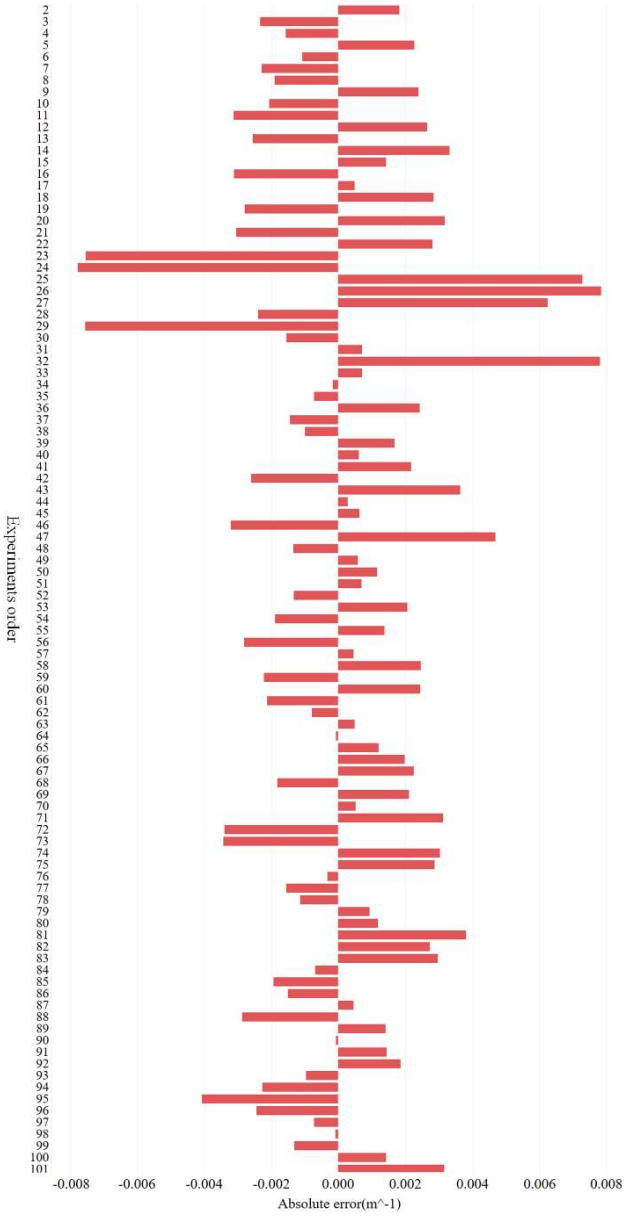

FIGURE 7. The absolute error of each experiment.

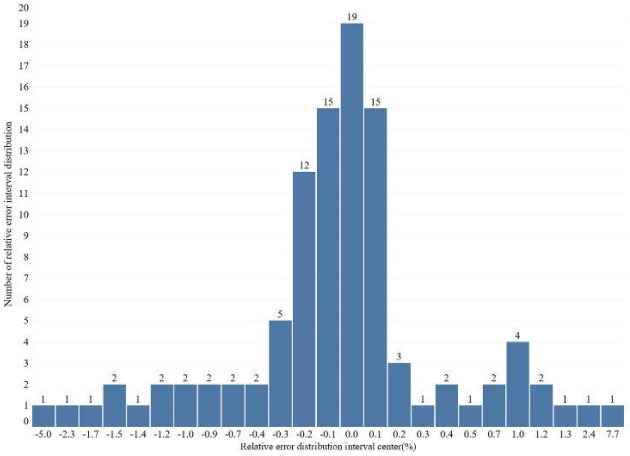

FIGURE 8. Relative error distribution.

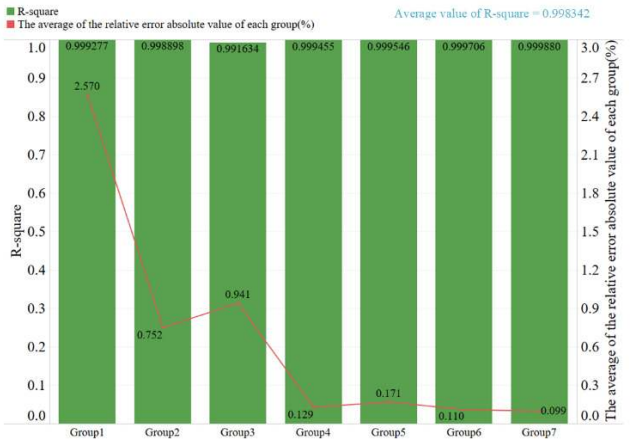

FIGURE 9. The R-square value and the average of the relative error absolute value of each group.

TABLE 5. Comparison between the proposed curvature demodulation method and related research.

Reference	Fitting physical quantity	Fitting type	Curvature ranges(m^{-1})
[19]	Light intensity	Linear equation	0.387-1.285
[20]	Light intensity	Linear equation	0-0.4
[22]	Wavelength	Linear equation	0-0.3
[25]	Wavelength	Linear equation	0.2-0.55 and 0.6-0.9
[26]	Wavelength	Linear equation	2.5-3.0
[27]	Wavelength	Linear equation	0-0.732
[29]	Wavelength	Linear equation	0.533-0.843
[30]	Wavelength	Linear equation	4.29-4.98 and 4.98-5.59
[31]	Wavelength	Linear equation	0-1.484
[32]	Wavelength	Linear equation	0-0.65
This paper	**All**	Matrix form	0-2.312

scholars believe that the curvature is related to the wavelength variation of the interference spectrum [23]–[33]. Based on the above discrepancy, this study conducted detailed research. The comparison between the proposed curvature demodulation method and related research is listed in Table 5. The word '**All**' in the table means a component that combines light intensity, wavelength and other quantities of their spectral curve. The table illustrates that the curvature demodulation method proposed in this paper extracts the complete spectral information. The main factor affecting the accuracy of this method is the demodulation accuracy of the demodulator. This method has a wide range of curvature measurements. Moreover, the method does not rely on the light intensity or wavelength of a particular point on the spectral curve to demodulate the curvature. Since the method extracts the complete information of the spectral curve, it can demodulate the curvature objectively. Finally, the method is simple in form and thus easy to implement in practical applications. These findings are unexpected and suggest that the curvature demodulation method has excellent performance and broad application prospects.

There are some explanations for these findings. The orthogonal decomposition of the spectral curve allows the complete spectral information to be retained in the fit coefficients (F). Each term of the fit coefficients (F) is the component of the spectral curve at the corresponding basis. This decomposition method maps spectral information to a multidimensional space. Multidimensional space reveals data information that cannot be characterized in low-dimensional space. The analysis of multidimensional spatial data using a multidimensional data processing method can keep information completely. The support vector machine has significant advantages in solving high-dimensional, nonlinear, and small-sample fitting problems. The support vector machine improved by the genetic algorithm is used to fit the multidimensional data, which greatly improves the fitting precision. The concept of orthogonal decomposition and the GA-SVM combination proposed in this paper can solve the problem of fiber sensing demodulation for various physical quantities based on spectral information.

The demodulation method proposed in this paper is a demodulation method based on the transmission spectrum curve of MZI sensors. This method can demodulate the modulation effect of the external physical quantity change on the transmission spectrum of MZI sensors. This method can be applied to the curvature demodulation process of MZI sensors with different structure types.

This paper has some deficiencies and limitations. Because this study is in its infancy, this paper only considered the curvature demodulation method of this particular sensor. The cross-effects of temperature and strain on the curvature of the sensor were not studied in this paper. Since the orthogonal bases for decomposing the spectral curve were infinite, only the main bases affecting the decomposition accuracy were selected for decomposition. In this paper, a simple linear kernel function was selected when using the support vector machine for fitting analysis. The linear kernel function is simple in structure but weak in fitting ability. This is also the reason that some experimental data have low fitting accuracy. For example, from the 23rd experiment to the 33rd experiment in Fig. 7, the fitting absolute error values were higher than others. Another reason for this phenomenon is that the spectral curve similarity of the above experiments is low. The readers can find this answer in Fig. 5(c).

Further studies that consider the above deficiencies will need to be undertaken. First, the researchers will examine the response of the sensor proposed in this paper to temperature or strain and the coupling law between them to curvature. Second, subsequent research will look for a set of orthogonal bases that are simple in structure, small in number, and suitable for most sensor spectral curves. Third, subsequent research will build a norm based on the orthogonal decomposition coefficients of the spectral curves. Subsequent research will look for an algorithm of this norm. The algorithm is used to characterize the relationship between curvature and relative changes in spectral information.

V. CONCLUSION

This study set out to construct a curvature demodulation method based on the complete spectral information of the MZI curvature sensor. The researchers chose some finite Chebyshev polynomials as the orthogonal bases to decompose the spectral curve. The coefficient of determination (R-square) after orthogonal decomposition of each spectral curve was greater than 0.999. The improved support vector machine by the genetic algorithm (GA-SVM) was used to fit the relationship between spectral curve decomposition coefficients and curvature. The average fitting accuracy of the demodulation method proposed in this paper reached 0.998342. The equivalent absolute error of the method proposed in this paper is 0.0022494 m^{-1}, which is superior to other methods. The demodulation method proposed in this paper extracts complete information about the sensor's full-band spectrum. Based on this advantage, the method can be used for the analysis and demodulation of spectral information for various optical sensors. The demodulation method proposed in this study has a broad range of applications. The important contribution of this research is to introduce the concept of orthogonal decomposition into the spectral information analysis of optical fiber sensing. The second innovation of this paper is that artificial intelligence algorithms (GA-SVMs) were used to fit and analyze multidimensional spectral information to improve the demodulation accuracy.

REFERENCES

[1] B. H. Lee, Y. H. Kim, K. S. Park, J. B. Eom, M. J. Kim, B. S. Rho, and H. Y. Choi, "Interferometric fiber optic sensors," *Sensors*, vol. 12, no. 3, pp. 2467–2486, Feb. 2012.

[2] P. Prerana, R. K. Varshney, B. P. Pal, and B. Nagaraju, "High sensitive fiber optic temperature sensor based on a side-polished single-mode fiber coupled to a tapered multimode overlay waveguide," *J. Opt. Soc. Korea*, vol. 14, no. 4, pp. 337–341, Dec. 2010.

[3] J. Y. Cho, J. H. Lim, and K. S. Lee, "Optical fiber twist sensor with two orthogonally oriented mechanically induced long-period grating sections," *IEEE Photon. Technol. Lett.*, vol. 17, no. 2, pp. 453–455, Feb. 2005.

[4] D. W. Kim, F. Shen, X. Chen, and A. Wang, "Simultaneous measurement of refractive index and temperature based on a reflection-mode long-period grating and an intrinsic Fabry–Pérot interferometer sensor," *Opt. Lett.*, vol. 30, no. 22, pp. 3000–3002, Nov. 2005.

[5] W.-S. Choi and M.-S. Jo, "Accurate Evaluation of polarization characteristics in the integrated optic chip for interferometric fiber optic gyroscope based on path-matched interferometry," *J. Opt. Soc. Korea*, vol. 13, no. 4, pp. 439–444, Dec. 2009.

[6] X. Wang, J. Xu, Y. Zhu, K. L. Cooper, and A. Wang, "All-fused-silica miniature optical fiber tip pressure sensor," *Opt. Lett.*, vol. 31, no. 7, pp. 885–887, Apr. 2006.

[7] W. Dong-Yuan, S. Ming-Ming, J. Yong-Xing, W. A. N. G. Jian-Feng, and D. O. N. G. Xin-Yong, "Simultaneous measurement of curvature and temperature based on optical fiber sensor," *Guangzi Xuebao/Acta Photonica Sinica.*, vol. 44, no. 11, Nov. 2015, Art. no. 1106004.

[8] M. Shao, X. Qiao, H. Fu, H. Li, J. Zhao, and Y. Li, "A Mach–Zehnder interferometric humidity sensor based on waist-enlarged tapers," *Opt. Lasers Eng.*, vol. 52, pp. 86–90, Jan. 2014.

[9] Y. Zhao, F. Xia, and J. Li, "Sensitivity-enhanced photonic crystal fiber refractive index sensor with two waist-broadened tapers," *J. Lightw. Technol.*, vol. 34, no. 4, pp. 1373–1379, Feb. 15, 2016.

[10] H. Wang, H. Meng, R. Xiong, Q. Wang, B. Huang, X. Zhang, W. Yu, C. Tan, and X. Huang, "Simultaneous measurement of refractive index and temperature based on asymmetric structures modal interference," *Opt. Commun.*, vol. 364, pp. 191–194, Apr. 2016.

[11] S. Korposh, S. W. James, S.-W. Lee, and R. P. Tatam, "Tapered optical fibre sensors: Current trends and future perspectives," *Sensors*, vol. 19, no. 10, p. 2294, May 2019.
[12] L. Li, L. Xia, Z. Xie, and D. Liu, "All-fiber Mach–Zehnder interferometers for sensing applications," *Opt. Express*, vol. 20, no. 10, pp. 11109–11120, May 2012.
[13] Y. Zhao, F. Xia, and M.-Q. Chen, "Curvature sensor based on Mach–Zehnder interferometer with vase-shaped tapers," *Sens. Actuators A, Phys.*, vol. 265, pp. 275–279, Oct. 2017.
[14] M. Deng, C.-P. Tang, T. Zhu, and Y.-J. Rao, "Highly sensitive bend sensor based on Mach–Zehnder interferometer using photonic crystal fiber," *Opt. Commun.*, vol. 284, no. 12, pp. 2849–2853, Jun. 2011.
[15] L. Mao, P. Lu, Z. Lao, and D. Liu, "In-fiber Mach–Zehnder interferometer based on multi-mode fiber and up-taper for curvature sensing," *Optik*, vol. 125, no. 18, pp. 5108–5111, Sep. 2014.
[16] H. S. Lin, Y. M. Raji, J. H. Lim, S. K. Lim, M. R. Mokhtar, and Z. Yusoff, "Packaged in-line Mach–Zehnder interferometer for highly sensitive curvature and flexural strain sensing," *Sens. Actuators A, Phys.*, vol. 250, pp. 237–242, Oct. 2016.
[17] Q. Wang and Y. Liu, "Review of optical fiber bending/curvature sensor," *Measurement*, vol. 130, pp. 161–176, Dec. 2018.
[18] H. Sun, S. Yang, X. Zhang, L. Yuan, Z. Yang, and M. Hu, "Simultaneous measurement of temperature and strain or temperature and curvature based on an optical fiber Mach–Zehnder interferometer," *Opt. Commun.*, vol. 340, pp. 39–43, Apr. 2015.
[19] Y. Zhao, M.-Q. Chen, F. Xia, L. Cai, and X.-G. Li, "Small curvature sensor based on butterfly-shaped Mach–Zehnder interferometer," *IEEE Trans. Electron Devices*, vol. 64, no. 11, pp. 4644–4649, Nov. 2017.
[20] F. Xia, Y. Zhao, and M. Chen, "Optimization of Mach–Zehnder interferometer with cascaded up-tapers and application for curvature sensing," *Sens. Actuators A, Phys.*, vol. 263, no. 11, pp. 140–146, Aug. 2017.
[21] Y. M. Raji, H. S. Lin, S. A. Ibrahim, M. R. Mokhtar, and Z. Yusoff, "Intensity-modulated abrupt tapered fiber Mach–Zehnder interferometer for the simultaneous sensing of temperature and curvature," *Optics Laser Technol.*, vol. 86, pp. 8–13, Dec. 2016.
[22] B. Jiang, Z. Bai, C. Wang, Y. Zhao, J. Zhao, L. Zhang, and K. Zhou, "In-line Mach–Zehnder interferometer with D-shaped fiber grating for temperature-discriminated directional curvature measurement," *J. Lightw. Technol.*, vol. 36, no. 3, pp. 742–747, Feb. 1, 2018.
[23] P. Wang, X. Shu, Y. Kong, Z. Xu, and Q. Yu, "Femtosecond direct writing of intergrated Mach–Zehnder interferometer with Bragg grating for curvature-temperature discrimination," in *Proc. Asia Commun. Photon. Conf. (ACP)*, Hangzhou, China, Oct. 2018, pp. 1–4.
[24] Q. Meng, Z. Chen, X. Dong, and K. Ni, "Simultaneous measurement of curvature and temperature based on two waist-enlarged fiber tapers and a fiber Bragg grating," in *Proc. Photonics Global Conf. (PGC)*, Singapore, Dec. 2012, pp. 1–5.
[25] H. Li, H. Li, F. Meng, X. Lou, and L. Zhu, "All-fiber MZI sensor based on seven-core fiber and fiber ball symmetrical structure," *Opt. Lasers Eng.*, vol. 112, pp. 1–6, Jan. 2019.
[26] T. Liu, H. Zhang, B. Liu, X. Zhang, H. Liu, and C. Wang, "Highly compact vector bending sensor with microfiber-assisted Mach–Zehnder interferometer," *IEEE Sensors J.*, vol. 19, no. 9, pp. 3343–3347, May 2019.
[27] H. Li, H. Li, X. Lou, F. Meng, and L. Zhu, "Soft optical fiber curvature sensor for finger joint angle proprioception," *Optik*, vol. 179, pp. 298–304, Feb. 2019.
[28] S. Wang, C. Shan, J. Jiang, K. Liu, X. Zhang, Q. Han, J. Lei, H. Xiao, and T. Liu, "Temperature-insensitive curvature sensor based on anti-resonant reflection guidance and Mach–Zehnder interferometer hybrid mechanism," *Appl. Phys. Express*, vol. 12, no. 10, Oct. 2019, Art. no. 106503.
[29] M. Xie, H. Gong, J. Zhang, C.-L. Zhao, and X. Dong, "Vernier effect of two cascaded in-fiber Mach–Zehnder interferometers based on a spherical-shaped structure," *Appl. Opt.*, vol. 58, no. 23, pp. 6204–6210, Aug. 2019.
[30] C. Zhang, J. Zhao, C. Miao, Z. Shen, H. Li, and M. Zhang, "High-sensitivity all single-mode fiber curvature sensor based on bulge-taper structures modal interferometer," *Opt. Commun.*, vol. 336, pp. 197–201, Feb. 2015.
[31] H. Song, H. Gong, K. Ni, and X. Dong, "All fiber curvature sensor based on modal interferometer with waist enlarge splicing," *Sens. Actuators A, Phys.*, vol. 203, pp. 103–106, Dec. 2013.
[32] X. Sun, H. Du, X. Dong, Y. Hu, and J. Duan, "Simultaneous curvature and temperature sensing based on a novel Mach–Zehnder interferometer," *Photon. Sensors*, pp. 1–10, May 2019.
[33] J. Cao, G. Lv, C. Chang, and H. Li, "A feature selection based serial SVM ensemble classifier," *IEEE Access*, vol. 7, pp. 144516–144523, 2019.
[34] M. Kafai and K. Eshghi, "CROification: Accurate kernel classification with the efficiency of sparse linear SVM," *IEEE Trans. Pattern Anal. Mach. Intell.*, vol. 41, no. 1, pp. 34–48, Jan. 2019.
[35] Y. Guo, X. Jia, and D. Paull, "Effective sequential classifier training for SVM-based multitemporal remote sensing image classification," *IEEE Trans. Image Process.*, vol. 27, no. 6, pp. 3036–3048, Jun. 2018.
[36] Z. Sun, K. Hu, T. Hu, J. Liu, and K. Zhu, "Fast multi-label low-rank linearized SVM classification algorithm based on approximate extreme points," *IEEE Access*, vol. 6, pp. 42319–42326, 2018.
[37] X. Wu, W. Zuo, L. Lin, W. Jia, and D. Zhang, "F-SVM: Combination of feature transformation and SVM learning via convex relaxation," *IEEE Trans. Neural Netw. Learn. Syst.*, vol. 29, no. 11, pp. 5185–5199, Nov. 2018.
[38] C. Sukawattanavijit, J. Chen, and H. Zhang, "GA-SVM algorithm for improving land-cover classification using SAR and optical remote sensing data," *IEEE Geosci. Remote Sens. Lett.*, vol. 14, no. 3, pp. 284–288, Mar. 2017.
[39] J. Wu and H. Yang, "Linear regression-based efficient SVM learning for large-scale classification," *IEEE Trans. Neural Netw. Learn. Syst.*, vol. 26, no. 10, pp. 2357–2369, Oct. 2015.
[40] X. Liu and J. Tang, "Mass classification in mammograms using selected geometry and texture features, and a new SVM-based feature selection method," *IEEE Syst. J.*, vol. 8, no. 3, pp. 910–920, Sep. 2014.
[41] A. Mathur and G. M. Foody, "Multiclass and binary SVM classification: Implications for training and classification users," *IEEE Geosci. Remote Sens. Lett.*, vol. 5, no. 2, pp. 241–245, Apr. 2008.
[42] Z. Long, X. Zhou, X. Zhang, R. Wang, and X. Wu, "Recognition and classification of wire bonding joint via image feature and SVM model," *IEEE Trans. Compon., Packag., Manuf. Technol.*, vol. 9, no. 5, pp. 998–1006, May 2019.
[43] S. Koda, A. Zeggada, F. Melgani, and R. Nishii, "Spatial and structured SVM for multilabel image classification," *IEEE Trans. Geosci. Remote Sens.*, vol. 56, no. 10, pp. 5948–5960, May 2018.
[44] S. Yu, X. Li, X. Zhang, and H. Wang, "The OCS-SVM: An objective-cost-sensitive SVM with sample-based misclassification cost invariance," *IEEE Access*, vol. 7, pp. 118931–118942, 2019.
[45] S. Yuan, "Research on fiber sensor based on the spherical-shape structure of SMF," M.S. thesis, Tianjin Univ. Technol., Tianjin, China, 2015.

MINGYAO LIU received the Ph.D. degree from the Shenyang Institute of Automation, Chinese Academy of Sciences, Shenyang, in 2002. He has presided over five national key projects. He has published more than 50 academic articles. His research interests include fiber-optic sensing, equipment condition monitoring, oil extraction equipment, robotics, and mechatronics.

JINGLIANG WANG received the master's degree from Huazhong Agricultural University, Wuhan, in 2016. He is currently pursuing the Ph.D. degree with the Wuhan University of Technology, Wuhan. His research interests include fiber-optic sensing, equipment condition monitoring, and deformation reconstruction.

YI LIU , photograph and biography not available at the time of publication

YUEGANG TAN , photograph and biography not available at the time of publication

KANG YUN received the B.S. degree in instrument science and technology from the Harbin Institute of Technology (HIT), Harbin, China, in 2004, and the M.Eng. degree in computer science from the Huazhong University of Science and Technology, Wuhan, China, in 2008. He is currently pursuing the Ph.D. degree with the School of Mechanical and Electronic Engineering, Wuhan University of Technology, Wuhan. His main research interests include optical fiber sensing and its applications and structure health monitoring.

LIU HONG, photograph and biography not available at the time of publication

HAN SONG, photograph and biography not available at the time of publication

XIANGSHENG ZENG, photograph and biography not available at the time of publication

PING XIA, photograph and biography not available at the time of publication

ZHAO LI, photograph and biography not available at the time of publication